20th IMEKO TC4 International Symposium and
18th International Workshop on ADC Modelling and Testing
Research on Electric and Electronic Measurement for the Economic Upturn
Benevento, Italy, September 15-17, 2014

Π-shifted fiber Bragg grating ring resonator as a splitting mode resonant sensor

Carlo Edoardo Campanella[1], Lorenzo Mastronardi, Francesco De Leonardis, Vittorio M.N. Passaro[2]

Photonics Research Group, Dipartimento di Ingegneria Elettrica e dell'Informazione,
Politecnico di Bari, Via E. Orabona 4, 70125 Bari, Italy
[1] edoardo.campanella81@gmail.com, [2] vittorio.passaro@poliba.it

***Abstract* – In this paper we report on a splitting mode resonant sensor based on a ring cavity formed by closing on itself a π-shifted fiber Bragg grating. In particular, this cavity allows to obtain a spectral response characterized by a splitting mode structure, composed by both symmetric and antisymmetric resonances. The modal splitting occurs very close to the Bragg wavelength, where the π-shifted fiber Bragg grating shows its transmission resonant maximum.**
In this region, for particular index modulation depths of the fiber Bragg grating, the linewidth of the two antysimmetrical modes suffers of an opposite behaviour because the symmetrical resonance linewidth is enlarged while the antisymmetrical resonance linewidth is reduced. Thus, we demonstrate that, near the Bragg wavelength, the splitting magnitude only depends on the index modulation depth of the fiber Bragg grating and it is independent from the device length. In this way, being the splitting magnitude insensitive to the length variations associated to any external perturbation, the proposed device can be used for those sensing applications requiring a sensing mechanism immune to the environmental noise sources.

I. INTRODUCTION

In the last decade Fiber Bragg gratings (FBGs) are become fundamental for an enumerable range of commercial sensing applications addressed to the aeronautics, automotive industry, structure monitoring, undersea oil exploration. biomechanics, rehabilitation engineering and many others. Due to their performance, together with the small size, chemical inertness, immunity to electromagnetic interference and multiplexing capability, this kind of sensors is largely used to measure various parameters such as strain, force, pressure, displacement, temperature, humidity, electrical field, refractive index, rotation, position, vibrations, radiation dose and many others. Although the commonly used high-resolution FBG sensors are based on Fabry-Perot configurations [1], more complex FBG structures, including π-phase shifted gratings [2], Moirè gratings [3] and chirped gratings [4], are more suited in certain applications, such as ultrasonic hydrophones for medical sensing, [5] geophysical surveys for measurements of seismic activity [6], where extremely sharp resonances allows ultra-high sensitivity and, in its turn, high-resolution measurements. Recently the operating principle of the splitting mode sensors have been demonstrated for sensing applications. Indeed, an splitting based sensing scheme has been experimentally proposed for improving the detection limit of the resonant optical cavity. With this scheme, a resonant cavity is able to sense and size a Nanoparticle (NP) by evaluating the coupling between the two degenerate counter-propagating modes generated by presence of the NP in the cavity [7]. This modal coupling appears as a doublet in the resonator transmission spectrum [7]. A self-referencing sensing scheme, based on a similar physical effect involving the resonance splitting, has also been exploited to investigate the response of an optofluidic ring resonator [8], where the self referencing sensing is based on the common-mode noise suppression achieved through using two coupled ring resonators.
Recently, the theoretical explanation and experimental demostration of a mode-splitting strain sensor formed by including a Fiber Bragg Grating (FBG) in a closed fiber loop, has been carried out [9] for sensing strain, temperature and group index. For not vanishing values of the FBG reflectivity, a split-mode resonant structure can be observed, due to the degeneracy removal of two counter-propagating modes. In particulare, the magnitude of the mode splitting has been used to sense the localized strain applied to the resonator in the FBG region, in a cavity-enhanced measurement system almonst immune to the environmental perturbations.
In [10] the features of a mode-splitting RI sensor based on a SOI Bragg grating ring resonator closed on itself

ISBN-14: 978-92-990073-2-7

have been investigated. The spectral response of the device shows a splitting magnitude equal to the PBG spectral extension that is almost insensitive to both fabrication tolerances and environmental perturbations. Another resonant cavity, formed by two vertically stacked SOI micro-ring resonators, has been reported in [11]. This device has been used as a biosensor, by exploiting the interaction of the two coupled resonators with a microfluidic ring channel in which flows the biological species to be analyzed. Indeed, the change of the coupling conditions between the two rings and the consequent splitting variation has been proposed for the selective biological sensing. In [12] the physics of a mode-splitting RI sensor based on a SOI Bragg grating ring resonator, operating in both linear and nonlinear regimes, has been reported. In linear regime, it behaves like reported in [11]. In nonlinear regime, the sensor resolution can be improved by exploiting the spectral deformation of the split mode-structure due to the excitation of the non linear effects in the SOI material system.

In this frame, we propose a device consisting of a ring resonator cavity made by enclosing a π-shifted Fiber Bragg grating on itself. Differently from the conventional FBG [9-10], the π-FBG shows a resonant maximum in the transmission curve, centered at the Bragg wavelength, giving rise to other physical effects which will be explored in this work. As it will be demonstrated in the following, this configuration allows a resonant sensing mechanism to be achieved, based on the measurement of the distance of two split modes, insensitive to the environmental noise sources and to the fabrication tolerances.

II. π-SHIFTED FIBER BRAGG GRATING RING RESONATOR

The proposed π-shifted Fiber Bragg Grating Ring Resonator (π-FBGRR) is sketched in Fig. 1 and has been modelled by the transfer matrix method and coupled mode theory [9-10]. As it is shown in Fig. 1, the linearly polarized optical field of a laser source (E_i) is launched in the optical fiber in order to excite the resonator modes via the evanescent coupler 1. One photodiode is placed at the end of coupler 2 (at the bottom of Fig. 1) in order to monitor the light output. The photodiode allows to observe the intra-cavity spectral response (i.e. $T=|E_o/E_{in}|^2$), analysing the signal associated with E_o. Each coupler is modelled as a lumped element by the following transfer matrix, having a unitary determinant if the insertion loss is neglected [13]:

$$\begin{bmatrix} E_{o1c} \\ E_{o2c} \end{bmatrix} = \begin{bmatrix} \tau & -ik \\ -ik & \tau \end{bmatrix} \begin{bmatrix} E_{i1c} \\ E_{i2c} \end{bmatrix} \quad (1)$$

where E_{i1c} E_{i2c} are the input amplitudes of each coupler, while E_{o1c}, E_{o2c} are the coupler outputs. τ and k are, respectively, the fractions of the optical amplitudes transmitted and coupled via the evanescent coupler.

The π-FBGRR is physically composed from one FBG closed on itself through a supplementar optical path which introduces a phase delay (Φ), equal to $\pi\lambda_B/(2\lambda)$ (with λ_B the Bragg wavelength), for each counter-propagating wave generated inside the ring cavity [9,10].

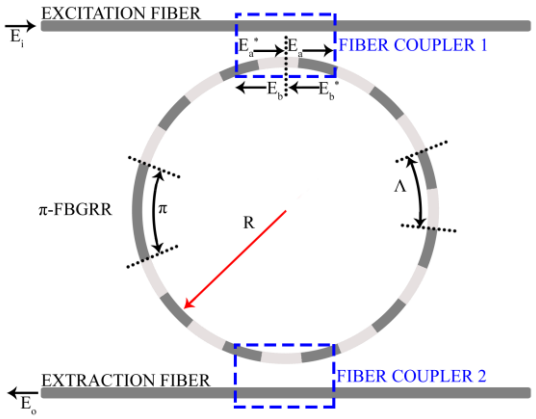

Fig.1: π-shifted Fiber Bragg Grating Ring Resonator (π-FBGRR) obtained by enclosing on itself a FBG through a supplementar optical path which introduces an overall phase delay of π between the two counter-propagating waves. The device is excited by an optical coupler 1 and the optical electric field is extracted by a fiber coupler 2.

Thus, with reference to a generic transversal section in the closed loop, by combining the relation reported in [9] and [14], the π-FBGRR can be modelled via a product of transfer matrices as:

$$\begin{bmatrix} E_a \\ E_b^* \end{bmatrix} = T_R \begin{bmatrix} e^{j\Phi} & 0 \\ 0 & e^{-j\Phi} \end{bmatrix} T_R \begin{bmatrix} E_a^* \\ E_b \end{bmatrix} = \begin{bmatrix} A_{11} & A_{12} \\ A_{21} & A_{22} \end{bmatrix} \begin{bmatrix} E_a^* \\ E_b \end{bmatrix} \quad (2)$$

where E_a, E_b^* and E_a^*,E_b represent the amplitudes of the electric fields incoming and outgoing from this generic section, respectively. T_R is a matrix expressed as:

$$T_R = \begin{bmatrix} t - r^2/t & r/t \\ -r/t & 1/t \end{bmatrix} \quad (3)$$

and t and r [10] result:

$$t = \frac{\Theta}{\Theta\cosh(\Theta\ell) + j\Delta\beta\sinh(\Theta\ell)}$$
$$r = \frac{jK\sinh(\Theta L)}{\Theta\cosh(\Theta\ell) + j\Delta\beta\sinh(\Theta\ell)} \quad (4)$$

with ℓ the FBG half length. Θ, K and $\Delta\beta$ can be expressed as:

$$\Theta = \left[|K|^2 - (\Delta\beta)^2 \right]^{\frac{1}{2}}; \; K = \frac{\pi |\Delta n|}{\lambda_B}; \; \Delta\beta = 2\pi n \left(\frac{\lambda_B - \lambda}{\lambda \lambda_B} \right); \tag{5}$$

where n is the effective index of the fiber, $|\Delta n|$, $\lambda_B = 2n \Lambda_B$ are the index modulation depth and the Bragg wavelength and Λ_B the FBG period, respectively.
These devices show a spectral response characterized by a photonic band gap (PBG) behavior, due to the fulfillment of the Bragg condition. The spectral extension of the Photonic Band Gap (PBG) is derived by considering the spectral region where the argument of Θ is real [10]. It is obtained when $\lambda_1 \le \lambda \le \lambda_2$, being:

$$\lambda_1 = \frac{2n\lambda_B}{2n + |\Delta n|}; \quad \lambda_2 = \frac{2n\lambda_B}{2n - |\Delta n|} \tag{6}$$

and it is given by:

$$\Delta\lambda_{PBG} = \lambda_1 - \lambda_2 = \left(\frac{4n|\Delta n|}{4n^2 - |\Delta n|^2} \right) \lambda_b = M \lambda_b \tag{7}$$

where M represents the magnitude of the PBG extension with respect to λ_B. To model the π-FBG behaviour, the following scattering matrix S is obtained from the transfer matrix of Eq. (2), like reported in [11]:

$$S = \begin{bmatrix} t_{\pi FBG} & -r_{\pi FBG} \\ -r_{\pi FBG} & t_{\pi FBG} \end{bmatrix} \tag{8}$$

with:

$$t_{\pi FBG} = \frac{t^2}{\left(r^2 + 1\right)} e^{j\Phi} \tag{9}$$

$$r_{\pi FBG} = \frac{r\left(t^2 - \left(r^2 + 1\right)\right)}{\left(r^2 + 1\right)} \tag{10}$$

Now, the spectral response of the device, T, can be derived by combining the matrix formalism as in [7], [11], by considering the elements of S matrix:

$$T = \left| \frac{E_o}{E_{in}} \right|^2 = \left| \frac{1}{2} \left[\frac{k^2 a \left(t_{\pi FBG} + r_{\pi FBG} \right)}{A_{22} - \tau^2 a^2 \left(t_{\pi FBG} + r_{\pi FBG} \right)} + \frac{k^2 a \left(t_{\pi FBG} - r_{\pi FBG} \right)}{A_{22} - \tau^2 a^2 \left(t_{\pi FBG} - r_{\pi FBG} \right)} \right] \right|^2 \tag{11}$$

where $a = \exp(-\alpha L)$ is the overall attenuation in a round trip due to the loss (α) per unit length and the right hand side of Eq. (11) is a combination of the two "symmetric" and "antisymmetric" guided wave solutions [9, 10, 16].
The symmetric resonant solutions of Eq. (11) can be evaluated by considering those wavelengths for which the denominator of the first term of Eq. (11) (i.e., f_S), given by:

$$f_S(\lambda) = 1 - \tau^2 a^2 \left[t_{\pi FBG}(\lambda) + r_{\pi FBG}(\lambda) \right] \tag{12}$$

vanishes, in order to satisfy the following dispersion equation:

$$1 = \tau^2 a^2 \left[t_{\pi FBG}(\lambda_{RS}) + r_{\pi FBG}(\lambda_{RS}) \right] e^{j2\pi q} \tag{13}$$

with λ_{RS} the eigen-modes of the system and q an integer (resonance order). The antisymmetric solutions can be found from the denominator of the second term of Eq. 11 (i.e., f_A):

$$f_A(\lambda) = 1 - \tau^2 a^2 \left[t_{\pi FBG}(\lambda) - r_{\pi FBG}(\lambda) \right] \tag{14}$$

and the antisymmetric dispersion equation is satisfied for λ_{RA} as:

$$1 = \tau^2 a^2 \left[t_{\pi FBG}(\lambda_{RA}) - r_{\pi FBG}(\lambda_{RA}) \right] e^{j2\pi q} \tag{15}$$

The splitting magnitude is the spectral distance between the resonance wavelengths λ_{RS} and λ_{RA}, evaluated for the same resonance order $q=q^*$. It can be expressed as:

$$Splitting = |\lambda_{RS} - \lambda_{RA}|_{q=q^*} \tag{16}$$

As reported in [11], in the spectral region where $t \neq 1$, the combination of the symmetric and antisymmetric solutions of Eq. (11) is responsible of a spectral behavior characterized by a splitting mode structure. In this spectral range, the split modes are a consequence of the degeneration removal of the two counter-propagating resonant modes coupled via FBG. Otherwise, for $t \approx 1$ in Eq. (11) the symmetric and antisymmetric solutions are quasi-degenerate and the values assumed from Eq. (16) approach to zero.
To describe the physical behavior of the device, we consider the physical parameters reported in Table I, whose assumed values are usual for fiber optics technology. In particular, the excitation and extraction fibers are conventional Single Mode Fiber (SMF), while the π-FBGRR parameters are those usually used in manifacturing the FBGs (i.e., $\lambda_B = 1.5605$ μm with a $|\Delta n|$ in the range $10^{-6} \div 10^{-5}$). With the same values assumed as in Table I, in Fig. 2 (a) the transmission curves, obtained by changing $|\Delta n|$ from 4×10^{-6} to 1×10^{-5} with a step of 2×10^{-6},

are reported.

Table I. Physical parameters and assumed values

Parameters	Assumed values
n (SMF)	1.457
$\|\Delta n\|$	4×10^{-6}, 6×10^{-6}, 8×10^{-6}, 1×10^{-5}, Fig. 2(a); $1\times10^{-6} \div 1\times10^{-5}$, Fig. 2(b), 3(a); 6×10^{-6}, Fig. 3(b);
λ_B	1.5605 μm
Λ	535.518 nm, Fig. 2(a), 3(a); 535.518 nm ÷ 535.524 nm, Fig. 3(b);
ℓ	2 cm
α	0.45×10^{-5} m^{-1}
τ	0. 975
k	$(1-\tau^2)^{1/2}$

A spectral range near the Bragg wavelength [1.56048 μm, λ_B=1.56050 μm] has been chosen. In this spectral region, the combination of the symmetric (Sym) and antisymmetric (Antisym) solutions of Eq. (11) is responsible of a spectral behaviour characterized by a splitting mode structure.

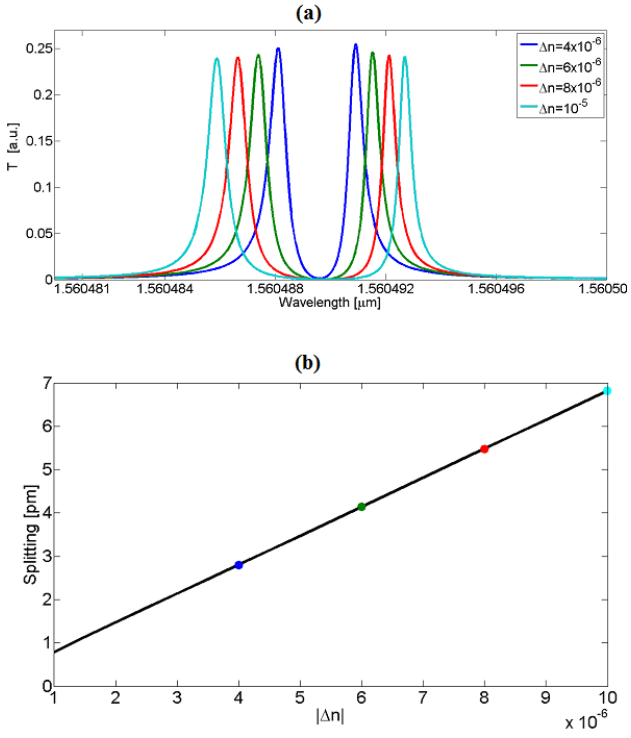

Fig.2:(a) Transmission (T) curves evaluated by changing $|\Delta n|$ from 4×10^{-6} to 1×10^{-5} with a step of 2×10^{-6} in the λ-range [1.56048 μm, 1.56050 μm]; (b) Splitting magnitude evaluated numerically by changing $|\Delta n|$ from 1×10^{-6} to 1×10^{-5} with a step of 1×10^{-7}.

The split modes are a consequence of the degeneration removal of the two counter-propagating resonant modes coupled via the π–FBG. In Fig. 2(b) the distance between the split resonant modes (i.e. *Splitting [pm]*, as reported in Eq. 16), has been numerically evaluated for $|\Delta n|$ ranging from 1×10^{-6} to 1×10^{-5}. With these physical parameters, the maximum achivable splitting is equal to 7 pm when $|\Delta n|=10^{-5}$.

Again with reference to Table I, in the same spectral range of Fig. 2(a), the transmission contour curve (T) obtained with a resolution of 5×10^{-7} is reported in Fig 3(a) by changing $|\Delta n|$ in the same interval of Fig. 2(b).

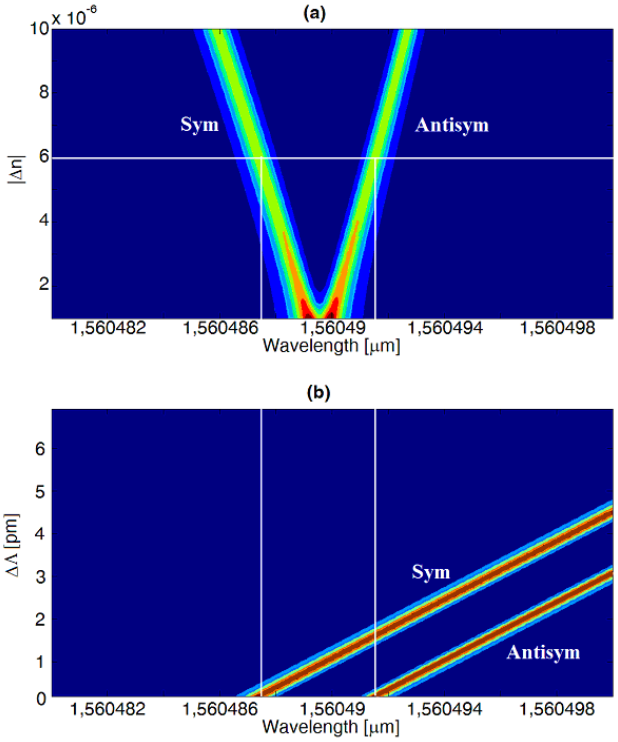

Fig.3: Transmission (T) contour curve in the λ-range [1.56048 μm, 1.5605 μm]; (a) evaluated with Λ=535.518 nm by changing $|\Delta n|$ from 1×10^{-6} to 1×10^{-5} with a resolution of 5×10^{-7}; (b) evaluated with $|\Delta n|=6\times10^{-6}$ by changing Λ from 535.518 nm to 535.524 nm with a resolution of 0.01 pm.

The 3D visualization gives more informations about the split modes behaviour. In fact, the symmetrical and antisymmetrical solutions of Eq. 11 cross each other for $|\Delta n|=0$, giving rise to the conventional mode resonance of a ring resonator. Otherwise, for small values of $|\Delta n|$ (i.e. $|\Delta n|=1\times10^{-6}$), a quasi degenerate split doublet appears. The splitting magnitude increases by increasing the index modulation depth $|\Delta n|$. Moreover, by increasing $|\Delta n|$, the linewidth of the two antysimmetrical modes suffers of an opposite behaviour because the symmetrical resonance linewidth is enlarged while the antisymmetrical resonance linewidth is reduced.

Now, in the same spectral range of Fig. 3(a), by fixing $|\Delta n| = 1\times10^{-6}$, we trace the transmission contour curve (T) by changing of 7 pm the initial value of the period Λ (i.e., in the Λ-range [535.518 nm, 535.524 nm] with a resolution of 0.01 pm). Although the period Λ changes of $\Delta\Lambda$, by inducing a shift of the split doubled of $\Delta\lambda_B$, the splitting magnitude still remains constant. This can be physically explained with reference to Eq. (7).

Like the extension of the PBG (i. e. M) is only shifted of $\Delta\lambda_B$ when Λ is varied of $\Delta\Lambda$, the splitting magnitude of the doublet suffers from the same wavelength shift. In fact, the splitting effect can be seen like a new PBG, generated from the scattered light inside the π-FBGRR, which preserves the same characteristics of the originary PBG, due to the scattered light in the π-FBG. Indeed, the π-FBG can be considered as a defective PBG device where the defect is introduced by the phase delay ($\Phi=\pi$). This results in a photonic localization state leading to the formation of a defect band (i.e., where the π-FBG shows the transmission maximum) and mini-PBGs within the mini defect band. Thus, the splitting effect represents a mini-PBG in the defect band. A physical analogy with this physical effect, regarding coupled-resonator optical waveguides (CROWs), can be found in [17].

III. CONCLUSIONS

In this paper we investigated a split mode resonant sensors based on a π-shifted fiber Bragg grating closed on itself. In this system, the overall scattering effect, due to the presence of the π-shifted fiber Bragg grating, creates two counter-propagating optical beams, coupled via the grating effect. To describe the physical behavior of the system, we adopt a general model and consider the conventional physical parameters of the fiber optics technology. The eigen-modes of the system, represented by symmetric and anti-symmetric resonant solutions cross each other in degenerate mode condition. The degenerate mode condition occurs at the Bragg wavelength for a weak index modulation depth $|\Delta n|=1\times10^{-6}$. Otherwise, by increasing $|\Delta n|$, the two antysimmetrical modes are not degenerate and their linewidth suffers of an opposite behaviour because the symmetrical resonance linewidth is enlarged while the antisymmetrical resonance linewidth is reduced. If the period of the π-shifted fiber Bragg grating changes of a small quantity, by inducing a shift of the split doubled, the splitting magnitude remains constant.

Thus, we can conclude that, being the splitting magnitude insensitive to the length variations associated with the external perturbations, the proposed device can be used for those sensing applications (i.e. strain/ temperature and many others), requiring a sensing mechanism immune to the environmental noise sources.

We believe that this system has strong potential for the spectroscopic sensing and may find innumerable applications also in the fields of opto-mechanics, quantum optics, physics of light-matter interactions and many others.

Moreover, the proposed principle could be taylored to the integrated optics technology with the advantage of obtaining miniaturized photonic sensors [18-19] with high immunity to both environmental noises and fabrication tolerances.

REFERENCES

[1] G. Gagliardi, M. Salza, S. Avino, P. Ferraro, P. De Natale, “Probing the Ultimate Limit of Fiber-Optic Strain Sensing,”, Science, vol. 330, 2010, pp. 1081-1084.

[2] Q. Wu and Y. Okabe, "High-sensitivity ultrasonic phase-shifted fiber Bragg grating balanced sensing system," Optics Express, vol. 20, 2012, pp. 28353-28362

[3] A. M Gillooly, L. Zhang, and I. Bennion “Quasi-distributed strain sensor incorporating a chirped Moire´ fiber Bragg grating,” IEEE Photonics Technology Letters, vol. 17, 2005, pp. 444-446.

[4] M. Pisco, A. Iadicicco, S. Campopiano, A. Cutolo, A. Cusano, “Structured Chirped Fiber Bragg Gratings,” J. Lightwave Technology, vol. 26, 2008, pp. 1613-1625.

[5] N. E. Fisher , D. J. Webb , C. N. Pannell , D. A. Jackson , L. R. Gavrilov , J. W. Hand , L. Zhang , I. Bennion “Ultrasonic hydrophone based on short in-fiber bragg gratings,” Applied Optics, vol. 37, 1998, pp. 8120-8128.

[6] P. Ferraro and P. De Natale, "On the possible use of optical fiber Bragg gratings as strain sensors for geodynamical monitoring," Optics & Laser Engineering, vol. 37, 2002, pp. 115-130.

[7] J. Zhu, S. K. Ozdemir, Y. F. Xiao, L. Li, L. He, D. R. Chen, and L. Yang, “On-chip single nanoparticle detection and sizing by mode splitting in an ultrahigh-Q microresonator,” Nature Photonics, vol. 4, 2010, pp. 46-49.

[8] M. Li, X. Wu, L. Liu, X. Fan, and L. Xu, “Self-Referencing Optofluidic Ring Resonator Sensor for Highly Sensitive Biomolecular Detection,” Anal. Chem., vol. 85, 2013, pp. 9328–9332.

[9] C. E. Campanella, A. Giorgini, S. Avino, P. Malara, R. Zullo, G. Gagliardi, and P. De Natale, “Localized strain sensing with fiber Bragg-grating ring cavities,” Optics Express, vol. 21, 2013, pp. 29435-29441.

[10] C. E. Campanella, F. De Leonardis and V. M. N. Passaro, “Performance of Bragg grating ring resonator as high sensitivity refractive index sensor,” IEEE Proceedings of Fotonica 2014, May 12th-14th, 2014, Naples (Italy).

[11] C. E. Campanella, C. M. Campanella, F. De Leonardis, and V. M. N. Passaro, “A high efficiency label-free photonic biosensor based on vertically stacked ring resonators,” in publication on European Physical Journal- Special Topics, 2014.

[12] F. De Leonardis, C. E. Campanella, B. Troia, A. G. Perri, and V. M. N. Passaro, “Performance of SOI Bragg Grating Ring Resonator for Nonlinear Sensing Applications,” in publication on Sensors, 2014.

[13] A. Yariv, “Universal relations for coupling of optical power between microresonators and dielectric waveguides,” Electron. Lett., vol. 36, 2000, pp. 321-324.

[14] E. Turan, “Fiber Grating Spectra,” J. Lightwave Technology, vol. 15, 1997, pp. 1277-1294.

[15] J. M. Choi, R. K. Lee, A. Yariv, “Ring fiber resonators based on fused-fiber grating add–drop filters: application to resonator coupling,” Opt. Lett., vol. 27, 2002, pp. 1598-1600.

[16] J. Ctyroky, I. Richter, and M. Sinor, “Dual resonance in a waveguide coupled ring micro-resonator,” Opt. Quantum Electron., vol. 38, 2006, pp. 781-793.

[17] T. Y. L. Ang, M. K. Chin, “The effects of periodic and quasi-periodic orders on the photonic bandgap structures of microring coupled-resonator optical waveguides”, Optics Express, vol. 17, 2009, pp. 5176-5192

[18] M. La Notte, B. Troia, T. Muciaccia, C. E. Campanella, F. De Leonardis, V. M. N. Passaro, “Recent Advances in Gas and Chemical Detection by Vernier Effect-Based Photonic Sensors,” Sensors, vol. 14, 2014, pp. 4831- 4855.

[19] V. M. N. Passaro, C. De Tullio, B. Troia, M. La Notte, G. Giannoccaro, F. De Leonardis, “Recent Advances in Integrated Photonic Sensors,” Sensors, vol. 12, 2012, pp. 15558-15598.